

In-plane optical spectra of $Y_{1-x}Ca_xBa_2Cu_3O_{7-\delta}$: Overdoping and disorder effect on residual conductivity

E. Uykur, K. Tanaka, T. Masui, S. Miyasaka, and S. Tajima

Department of Physics, Graduate School of Science, Osaka University, Osaka 560-0043, Japan

We measured the temperature dependence of the in-plane polarized reflectivity spectra of twin-free $Y_{1-x}Ca_xBa_2Cu_3O_{7-\delta}$ single crystals with different Ca-concentrations ($x = 0, 0.11$ and 0.16) from optimally doped to heavily overdoped region. Low energy optical conductivity spectra showed a Drude-like residual conductivity at temperatures far below the superconducting transition temperature, which indicates the presence of unpaired-normal carriers in the superconducting state. Comparing the spectra at a fixed Ca-content or at a fixed doping level, we have revealed that the carrier overdoping increases unpaired carriers in addition to those induced by the Ca-disorder. We also found the superconducting behavior of the one-dimensional CuO chains for the Ca-free samples.

PACS numbers: 74.25.Gz, 74.72.-h

Keywords: (Y,Ca)Ba₂Cu₃O_{7- δ} , far-infrared, in-plane optical spectra, chain conductivity

INTRODUCTION

The overdoped regime of cuprate superconductors has not been intensively investigated, compared to the well studied pseudogap phase in the underdoped regime [1], although many unresolved problems remain in the former. One of the reasons for this situation is that it is believed that in the overdoped regime, the system is approaching a conventional Fermi liquid state and thus nothing peculiar happens. The other is a technical reason that only limited materials such as Tl-based cuprates can achieve the overdoped state.

Among some anomalies in the overdoped regime, we focus here on the low energy optical response. When the system goes into the superconducting state with d -wave symmetry, the optical conductivity is suppressed below the gap energy (2Δ) and gradually decreases towards zero at $\omega = 0$. However, in many cuprates, a substantial amount of conductivity remains finite at $\hbar\omega \ll 2\Delta$, forming a Drude-like spectrum even at $T \approx 0$. This residual conductivity suggests the presence of unpaired normal carriers in the superconducting state. Impurity pair-breaking could be one of the sources for this residual conductivity, since Zn-doped cuprates exhibit a similar low frequency response [2]. The problem is that this anomaly can be observed even in impurity-free samples [3]. Its origin is unknown.

The increase of the residual conductivity with carrier overdoping was first reported in the c -axis spectra of $YBa_2Cu_3O_{7-\delta}$ (Y-123) [4, 5] and $Y_{1-x}Ca_xBa_2Cu_3O_{7-\delta}$ (Y/Ca-123) [6], followed by the study of the in-plane spectra of $Tl_2Ba_2CuO_{6+\delta}$ [7]. It seems to be related to overdoping, but not conclusive because disorder-induced pair-breaking cannot be ignored in most cases. For example, Ca-substitution for Y in $YBa_2Cu_3O_{7-\delta}$ lowers the maximum T_c value presumably because it introduces disorders into the CuO₂-planes, while it also introduces carrier-holes into the system. Therefore, we need to distinguish the effects of carrier-overdoping and Ca-disorder

in order to discuss the origin of residual conductivity.

So far, there have been few studies for the in-plane optical spectra of overdoped cuprates except for $Tl_2Ba_2CuO_{6+\delta}$ (Tl2201) and $Bi_2Sr_2CaCu_2O_{8+\delta}$ (Bi2212)[7, 8]. In the present work, we prepared detwinned single crystals of $Y_{1-x}Ca_xBa_2Cu_3O_{7-\delta}$ for various Ca- and oxygen-contents. In order to separate the effects of overdoping and Ca-disorder, we studied the spectral change with Ca-content by fixing the doping level, as well as the change with doping by fixing the Ca-content. These comparisons have revealed that overdoping definitely increases the unpaired carriers. While Ca-substitution also enhances residual conductivity, its effect is weaker than the Zn-substitution effect.

Moreover, for highly oxygenated Y-123, we observed a clear conductivity suppression due to the superconducting gap opening in the Cu-O chain spectra. It seems that the decrease of oxygen deficiency leads to high conductivity in the chains and thus to a superconducting response.

EXPERIMENTS AND SAMPLE CHARACTERIZATION

$Y_{1-x}Ca_xBa_2Cu_3O_{7-\delta}$ single crystals (for $x = 0, 0.11$ and 0.16) were grown by using a pulling technique explained elsewhere [9]. As-grown crystals were cut into pieces with ab -plane surfaces that were not smaller than 4×4 mm². Then the pieces were detwinned under uniaxial pressure (~ 8 kg/mm²). For reflectivity measurements, the sample surfaces were mechanically polished by using Al₂O₃ powder gradually as fine as 0.3 μ m. To obtain optimally doped crystals, samples were annealed at 500 and 575 °C for $x = 0$ and $x = 0.11$, respectively, in an oxygen atmosphere for about 1 month. For the overdoped region, all samples were annealed at 350 °C under oxygen flow for about 2 months. The superconducting transition temperatures were determined by the dc susceptibility measurements as follows: 93.5 and 87

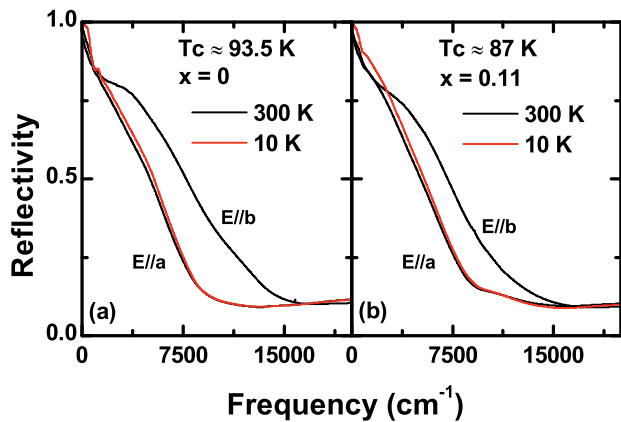


FIG. 1. The polarized in-plane reflectivity spectra in the optimally doped samples with (a) $x = 0$ and (b) $x = 0.11$.

K for $x = 0$ and $x = 0.11$, respectively, in the optimally doped regime, while in the overdoped region, T_c values decreased down to 90 K for $x = 0$, 75 K for $x = 0.11$, and 70 K for $x = 0.16$. The doping levels (p) were determined from T_c , assuming the empirical formula between p and T_c [10]. DC resistivity was measured by a standard four probe method.

The temperature dependent reflectivity measurements were performed with a Bruker 80v Fourier transform infrared (FTIR) spectrometer from ~ 70 to ~ 20000 cm^{-1} with $E//a$ and $E//b$ polarizations at various temperatures from ~ 10 to ~ 300 K. The sample and the reference mirror (Au for far-infrared and middle infrared regions, Ag for near infrared and visible regions) were placed into a He-flow cryostat. Their spectra were compared successively at each measured temperature by checking their positions with a He-Ne laser. The optical conductivity spectra were obtained from the measured reflectivity spectra by using the Kramers-Kronig (K-K) transformation with the Hagen-Rubens extrapolation in the low-energy region. For the analysis, we used room-temperature reflectivity spectra in the higher-energy region up to 40 eV, which were measured with the use of synchrotron radiation at UV-SOR, Institute for Molecular Science (Okazaki). We also used ω^{-4} extrapolation above 40 eV.

Figures 1(a) and (b) show the in-plane polarized reflectivity spectra of the optimally doped crystals with $x = 0$ and 0.11 in a wide frequency range. The 10 K spectra are also given for $E//a$ to demonstrate that the appreciable temperature dependence is observed only in the low energy region. A clear a - b anisotropy can be seen both samples, which guarantees that our detwinning treatment was successful. The b -axis reflectivity edge for the Ca-substituted sample is located at lower energy compared to the Ca-free sample. This shift can be explained by the decrease of the carrier concentration in the

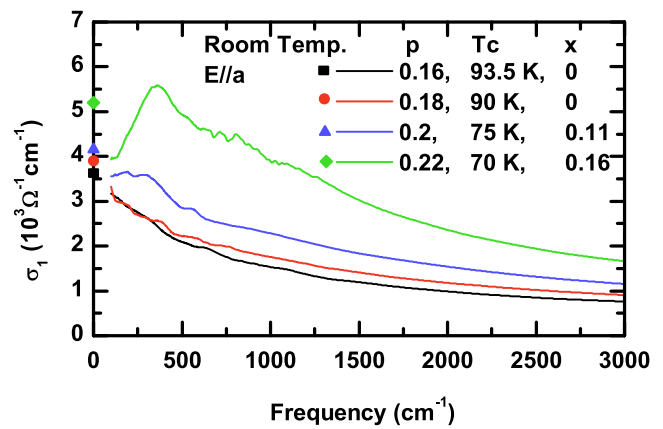


FIG. 2. Room temperature a -axis optical conductivity from $p = 0.16$ to $p = 0.22$. Solid symbols indicate the dc value for each sample.

chains, because in order to keep a constant doping level, we reduced the oxygen concentration in the chains for the Ca-substituted samples [11]. The estimated δ -values were 0.12 for $x = 0$ and 0.257 for $x = 0.11$, respectively.

RESULTS

Overdoping effect on a -axis residual conductivity

In the overdoped region, the samples with $x = 0$, 0.11, and 0.16 have been studied. The doping levels (p) were determined as 0.18, 0.2, and 0.22 for these samples, respectively. Figure 2 shows the comparison of the a -axis $\sigma_1(\omega)$ spectra at room temperature, together with the optimal doping spectrum for $x = 0$. The increase of the optical conductivity demonstrates a successful increase in carrier concentration. For the Ca-substituted samples, a peak-like structure evolves in the low-energy region (~ 300 cm^{-1}) in the normal state, which becomes more pronounced with increasing Ca-concentration. With decreasing temperature, this peak structure merges into the Drude-like conductivity. This feature is not only dependent of the Ca-content but also of the oxygen content. The origin of this Ca-induced peak is unknown at the moment.

With increasing carrier-doping, the characteristics of the optical spectra change dramatically. Figure 3 shows the reflectivity [(a)-(d)] and conductivity [(e)-(h)] spectra of the optimally doped sample with $x = 0$ and three overdoped samples with $x = 0$, 0.11, and 0.16, respectively. The conductivity spectra were calculated from the reflectivity spectra through the Kramers-Kronig (K-K) transformation. The low frequency conductivity can be smoothly connected to the dc values determined by dc resistivity measurement, which confirms the reliability of

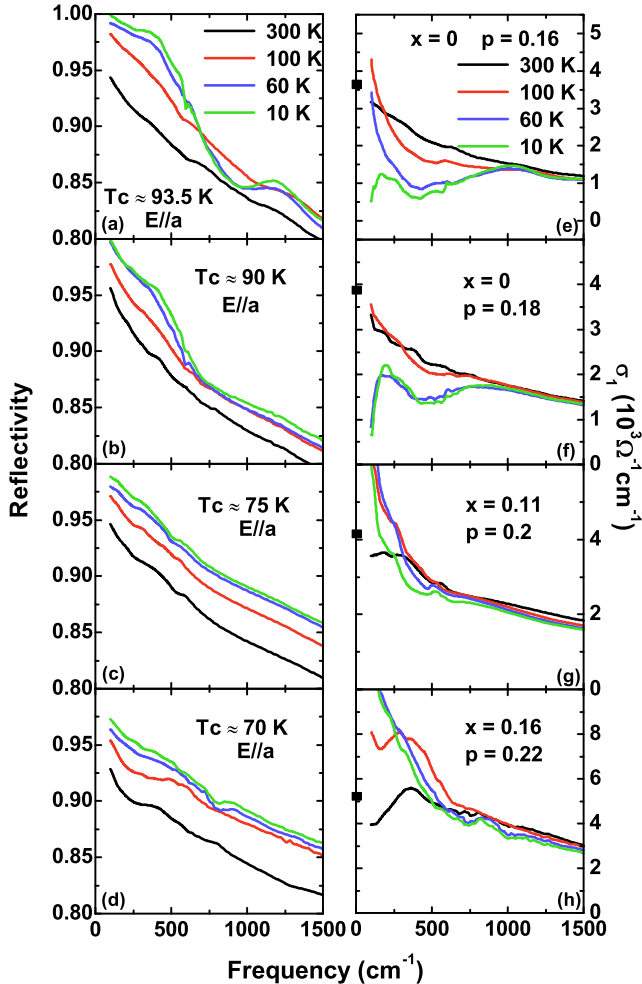


FIG. 3. Temperature dependent a -axis reflectivity spectra (left panels) of optimally doped sample with (a) $x = 0$ and three overdoped samples with (b) $x = 0$, (c) $x = 0.11$, and (d) $x = 0.16$. Right panels show the corresponding optical conductivity spectra. (e) for (a), (f) for (b), (g) for (c), and (h) for (d), respectively. Solid symbols show the dc conductivity values at 300 K.

our K-K transformation. The spectra for the optimally doped sample with $x = 0$ are almost identical to the data published so far [2, 12, 13]. The major change with temperature occurs in the low energy region, as can be seen in Fig. 1. In the normal state, the reflectivity increases with lowering frequency, as expected in a metallic system. In the superconducting state, a well known step-like behavior [14–16] is seen below 1000 cm^{-1} .

This behavior is clearly seen in the optimally doped sample while it weakens with overdoping and is almost suppressed for the heavily overdoped sample. Moreover, the reflectivity below 200 cm^{-1} at 10 K becomes lower with increasing p and x , which implies an increase of

some absorption within the superconducting gap.

In the conductivity spectra, for the Ca-free sample, the σ_1 -suppression at low frequencies associated with the superconducting condensation can be seen while the suppression weakens in the overdoped sample [Fig. 3(f)]. With further increasing p ($p = 0.2$ and 0.22), a clear superconducting gap could not be observed, except for a small suppression of the conductivity, which indicates possible gapless superconductivity in this state. In this overdoped region, $\sigma_1(\omega)$ shows a distinct Drude-like increase toward $\omega = 0$. The Drude-like peak for $p = 0.22$ is broader than that for $p = 0.2$, which indicates the increase of the residual conductivity with doping, namely, the increase of the unpaired normal carriers. The calculated spectral weights ($SW = \int_{100}^{600} \sigma(\omega) d\omega$) of the residual part at 10 K are $4.31 \times 10^6 \text{ } \Omega^{-1} \text{ cm}^{-2}$, $8.01 \times 10^6 \text{ } \Omega^{-1} \text{ cm}^{-2}$, $19.92 \times 10^6 \text{ } \Omega^{-1} \text{ cm}^{-2}$, and $30.15 \times 10^6 \text{ } \Omega^{-1} \text{ cm}^{-2}$ for samples in Figs. 3(e), (f), (g), and (h), respectively.

The strong increase of residual conductivity in Fig. 3 seems to be the effect of carrier-overdoping. However, it is not obvious whether this is only due to overdoping or if the disorder introduced by Ca-substitution contributes. To extract the overdoping effect solely, we compare the spectra of optimally doped and overdoped samples with the same Ca-content. Figures 4(a) and (b) show the normal state (100 K) and superconducting state (10 K) $\sigma_1(\omega)$ in the optimally doped and in the overdoped region for $x = 0$ and 0.11 , respectively. For both Ca-contents, the missing area is reduced with carrier overdoping. For the Ca-free sample, the residual conductivity at the lowest temperature (10 K) is enhanced in the overdoped sample, compared to that of the optimally doped sample. For $x = 0.11$, this increase is more pronounced. As a result, the suppression due to superconducting transition is almost erased by the Drude-like increase of the conductivity. Since we can observe a similar increase of residual conductivity for two sets of samples with different Ca-content, it is concluded that the carrier-overdoping intrinsically enhances the residual conductivity.

Ca-substitution effect at the optimum doping

Since we work with the Ca-substituted samples, it is necessary to examine whether the Ca-disorder effect exists. Figure 5 is a comparison of the spectra of Ca-free and Ca-substituted samples with the same doping level ($p = 0.16$). In Figs. 5(a) and (b) we found that the step-like feature in the reflectivity spectrum is getting weaker with Ca-substitution. The reflectivity below $\sim 400 \text{ cm}^{-1}$ is slightly lower for the Ca-substituted sample, which indicates some absorption due to normal carriers.

Figures 5(c) and (d) are the corresponding optical conductivity spectra. Since the doping levels are the same ($p = 0.16$) in both samples, the differences can be at-

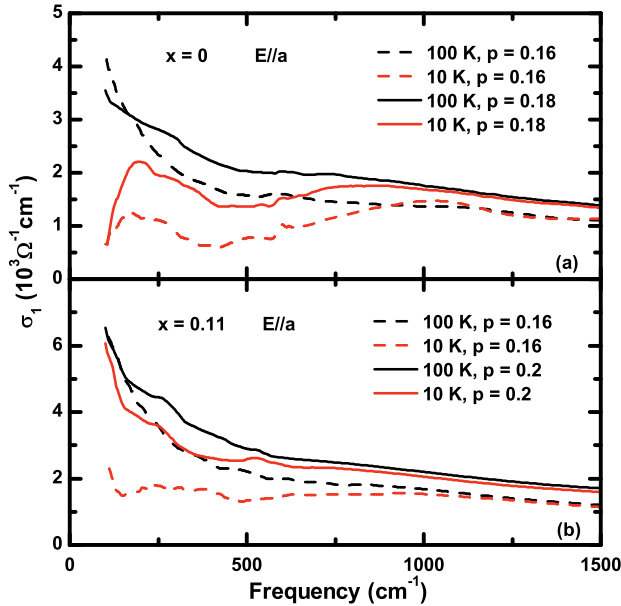


FIG. 4. Comparisons of a -axis optical conductivity in the normal state (100 K) and the superconducting state (10 K) for $\text{YBa}_2\text{Cu}_3\text{O}_{7-\delta}$ with (a) $x = 0$ and (b) $x = 0.11$. In both panels, the spectra of the optimally doped sample ($p = 0.16$) and the overdoped sample ($p = 0.18$ or $p = 0.2$) are compared.

tributed solely to the Ca-substitution effects. A noticeable change with Ca-substitution is seen in the superconducting state, while there is no substantial difference between the normal state spectra for $x = 0$ and 0.11. The suppression of the conductivity due to the superconducting condensation becomes weaker and the missing area decreases with Ca-substitution. Therefore, we conclude that the increase of residual conductivity and the decrease in the missing area are also caused by Ca-substitution, not only overdoping. Here it should be noted that the normal state spectra for the optimally doped samples do not appreciably change with Ca-substitution, which is consistent with the dc conductivity behavior.

b -axis spectra and the superconducting chain behavior

So far, we have focused on the a -axis spectra which give information about the two-dimensional CuO_2 planes. Next, we discuss the b -axis polarized spectra. b -axis measurements are also important for the Y-123 system to extract the chain contribution. Figures 6(a) and (d) show the low-frequency b -axis reflectivity spectra for the optimally doped and overdoped $\text{YBa}_2\text{Cu}_3\text{O}_{7-\delta}$, respectively, while Figs. 6(b) and (e) are the corresponding optical conductivity. The metallic behavior in the normal

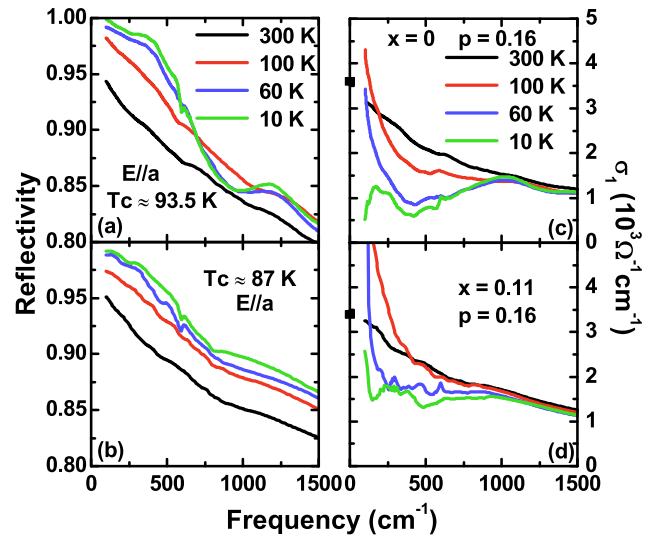


FIG. 5. Temperature dependent a -axis reflectivity spectra (left panels) in the optimally doped region for (a) $x = 0$ and (b) $x = 0.11$. Right panels show the corresponding optical conductivity spectra. Solid symbols show the dc conductivity values for 300 K.

state and the suppression of the conductivity with the superconducting transition can be seen as expected. The mid-infrared absorption due to disordered chains [17, 18] between $\sim 1000 \text{ cm}^{-1}$ and $\sim 3000 \text{ cm}^{-1}$ is shifting towards lower frequencies with overdoping. The b -axis conductivity values are higher than the a -axis values (Figs. 6(c) and (f)), which indicates the chain contribution to the optical conductivity.

The optical conductivity for the chain (σ_{CHAIN}) is estimated by subtracting the a -axis conductivity (σ_{1a}) from the b -axis one (σ_{1b}) as $\sigma_{\text{CHAIN}} = \sigma_{1b} - \sigma_{1a}$. Figures 7(a) and (b) show the chain conductivity in the optimally doped and overdoped sample, respectively. The conductivity in the disordered chains will occur with the hopping mechanism [19]. On the other hand, for the highly ordered chain structure, a metallic behavior can be expected. As support for this idea, we can see the shift of the mid-infrared absorption to lower energies and the development of a Drude-like spectrum in the chain response of the highly oxygenated sample. Moreover, at 10 K, a distinct suppression due to superconducting condensation can be observed. So far, although the higher conductivity in the b -axis spectra has been considered to indicate the contribution of the chains to the electronic conductivity, most of the reported chain spectra showed neither a Drude-like profile nor a superconducting response. Figure 7 demonstrates that with decreasing oxygen deficiency, the chains contribute to the superfluid density, as well. The superfluid response of the intrinsically metallic CuO chains would be the result of the proximity effect between chains and superconducting CuO_2 planes, which is theoretically predicted in Ref.

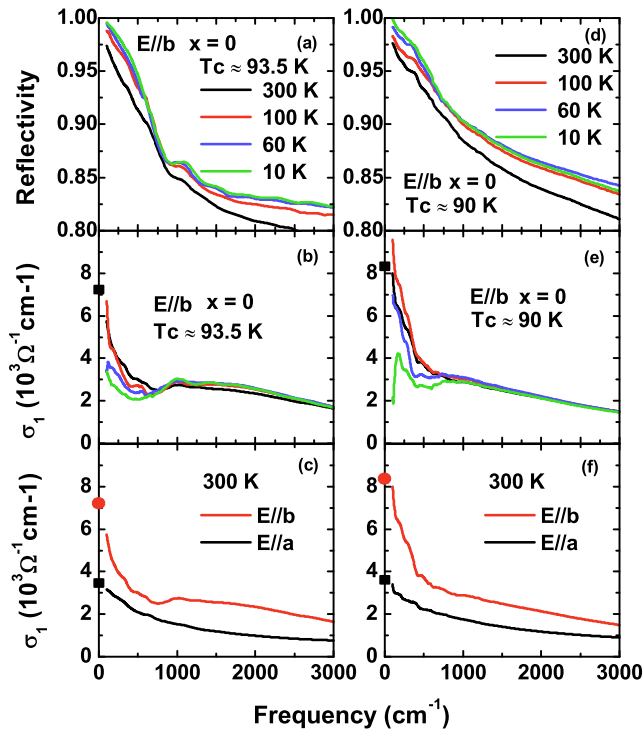


FIG. 6. Temperature dependent b -axis reflectivity spectra for $x = 0$ in the (a) optimally doped region and (d) overdoped region. (b) and (e) show the corresponding optical conductivity spectra for (a) and (d), respectively. (c) and (f) show the a -axis and b -axis optical conductivity in the room temperature. Solid symbols show the dc conductivity values at 300 K.

20. Although the missing area in the chain conductivity spectrum was reported for the oxygen deficient Y-123 in Ref. 21, we observed such a superconducting response only in the highly oxygenated Y-123.

Another possible source of the anisotropy of $\sigma_{1b} - \sigma_{1a}$ may be the stripe effect within the CuO_2 plane. A clear in-plane anisotropy was observed in the spectra of lightly doped $\text{La}_{2-x}\text{Sr}_2\text{CuO}_4$ [22] and $\text{YBa}_2\text{Cu}_3\text{O}_y$ [23], which was attributed to the nematic nature of the charge stripes. In Y-123, the CuO chain is supposed to play a role in alignment of the stripes, while it has almost no direct contribution to the conductivity. Compared to this data for the underdoped Y-123 [23], the magnitude of the difference $\sigma_{1b} - \sigma_{1a}$ is very large in the present result, which indicates a huge contribution of the CuO chain to the b -axis conductivity. Therefore, we believe that the anisotropy observed in this study is mainly caused by the CuO chain conductivity and the effect of the stripes, even if it exists, is much weaker than the chain conductivity.

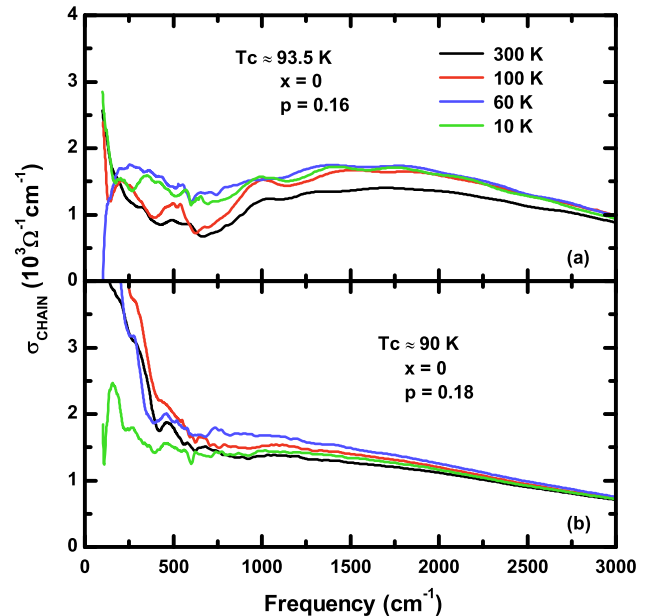


FIG. 7. Temperature dependent chain conductivity for $x = 0$ in the (a) optimally doped region and (b) overdoped region.

DISCUSSIONS

It is possible to calculate the superfluid density with two different methods. The first method is through the missing area of the a -axis optical conductivity. We calculated the missing area, $A = \int_{100}^{10000} [\sigma_{1n}(\omega) - \sigma_{1s}(\omega)] d\omega = c^2/8\lambda_L^2 = 4\pi n_s e^2/m^*$, using only reliable data down to 100 cm^{-1} for all the samples. Here, the spectra at 100 K and 10 K were used for $\sigma_{1n}(\omega)$ and $\sigma_{1s}(\omega)$, respectively. The obtained values for $\lambda_L^{-2} (\sim \omega_{ps}^2)$ are plotted in Fig. 8 as a function of the doping level (p). The second method is estimation from the imaginary part of the conductivity, $\sigma_2(\omega)$, which is equal to $\omega_{ps}^2/4\pi\omega$ at $\omega \ll 2\Delta$. The values obtained by the two methods are in good agreement with each other within the error bars in Fig. 8. The λ_L value for the optimally doped Ca-free sample was determined as 1520 \AA . This value is consistent with the reported data [2, 24]. In Fig. 8, we see a systematic decrease in superfluid density (n_s/m^*) with increasing p as well as with increasing Ca-concentration. Although there is an effect from Ca-substitution, as we showed in previous section, it is demonstrated that carrier overdoping is also an effective factor. Distinguishing the Ca-disorder effect from the overdoping effect, we can conclude that unpaired carriers are intrinsically induced by overdoping. The decrease of λ_L^{-2} with overdoping was also observed in muon spin rotation (μSR) measurements for Tl2201 [25, 26] and Ca-doped Y-123 [27], which suggests an electronic inhomogeneity in these systems.

Scanning tunnelling microscopy (STM) studies re-

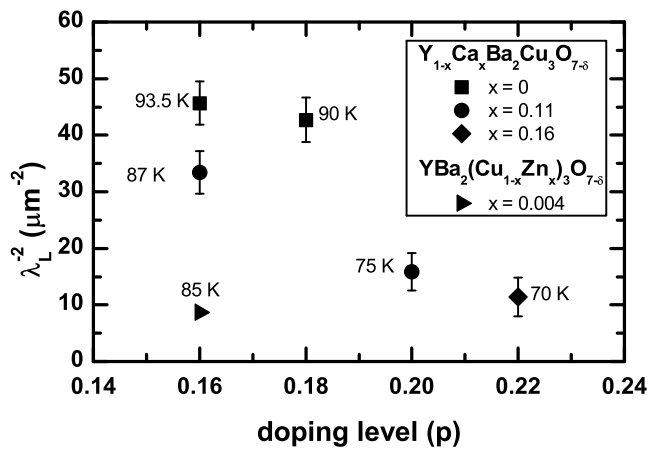


FIG. 8. The doping dependence of the superfluid density ($\sim \lambda_L^{-2}$) of $\text{Y}_{1-x}\text{Ca}_x\text{Ba}_2\text{Cu}_3\text{O}_{7-\delta}$ single crystals for $x = 0, 0.11$ and 0.16 . The \blacktriangleright shows the superfluid density of $\text{YBa}_2(\text{Cu}_{1-x}\text{Zn}_x)_3\text{O}_{7-\delta}$ for comparison (Ref. 2). Temperatures are T_c values for each sample.

vealed nanoscale spatial variations in the electronic state of the overdoped $\text{Bi}_2\text{Sr}_2\text{Cu}_2\text{O}_y$ [28, 29], contrary to many models of high temperature superconductors that consider electronically homogeneous systems. The increase of normal carriers in the superconducting state in the overdoped regime with increasing carrier density is also suggested by other methods. The loss of the specific heat anomaly and the increase in the zero-temperature specific heat coefficient [$\gamma(0)$] for $(\text{La,Sr})_2\text{CuO}_4$ and $\text{TlSr}_2\text{CaCu}_2\text{O}_{7-\delta}$ indicate the strong increase of unpaired carriers in the overdoped region [30]. In NMR measurements, the T-linear dependence of the nuclear spin-lattice relaxation rate ($1/T_1$) was observed at low temperatures in overdoped $\text{TlSr}_2\text{CaCu}_2\text{O}_{7-\delta}$, which was interpreted to reflect the existence of the residual density of states at the Fermi level, suggesting gapless superconductivity [31]. Moreover, recently the decrease of the Meissner volume fraction was observed on field cooling of the magnetic susceptibility measurements [32]. This indicates a decrease in superconducting carrier density due to the phase separation in the overdoped $(\text{La,Sr})_2\text{CuO}_4$.

Finally, we discuss the Ca-substitution effects on the scattering rate. The a -axis scattering rate was calculated by using the equation, $1/\tau(\omega) = \omega_p^2/4\pi \cdot \text{Re}(1/\sigma(\omega))$, as shown in Fig. 9. The ω_p values are determined with the Ferrell-Glover-Tinkham (FGT) sum rule by integration up to $\omega = 10000 \text{ cm}^{-1}$ as $\sim 1.66 \times 10^4 \text{ cm}^{-1}$, $\sim 1.69 \times 10^4 \text{ cm}^{-1}$, $\sim 1.92 \times 10^4 \text{ cm}^{-1}$, and $\sim 2.29 \times 10^4 \text{ cm}^{-1}$ for $x = 0$, $x = 0.11$ (optimally doped), $x = 0.11$ (overdoped), and $x = 0.16$, respectively. For the optimally doped sample with $x = 0$ (Fig. 9(a)), the normal state scattering rates show an almost linear increase with ω up to $\sim 3000 \text{ cm}^{-1}$. At the superconducting transition, a clear bump is formed around $\sim 1000 \text{ cm}^{-1}$ and the low ω scattering

rate is completely suppressed. This superconductivity-induced feature is getting weaker with Ca-substitution, as is expected from Fig. 5.

When the doping level is further increased, several changes are observed. First, the bump around $\sim 1000 \text{ cm}^{-1}$ vanishes gradually with the increasing doping level and the T -independent high frequency part becomes T -dependent (Figs. 9(c) and (d)). The disappearance of the bump feature is not only due to Ca-substitution but also due to overdoping (comparison of Figs. 9(b) and (c)). The second noticeable change is the decrease in scattering rate in spite of the increase of Ca-disorder. It is considered that the carrier doping effect overcomes the effect of disorder. Thirdly, the ω -dependence changes from ω -linear towards ω^2 -behavior. The latter is an indication of the Fermi liquid nature of the system. For the heavily overdoped region a small upturn is also observed below 500 cm^{-1} in Fig. 9(d), which becomes stronger with decreasing temperature. A similar behavior observed in the heavily overdoped region is discussed in detail for $\text{Bi}2212$ [33] and $\text{Tl}2201$ [7] systems. The upturn of the low energy scattering rate usually explained by the charge localization induced by impurity in disorder introduced systems or by local disordered octahedral distortion for the $\text{Tl}2201$ system.

The other important finding in Fig. 9 is that the scattering rate is insensitive to Ca-concentration. It is seen when we compare the spectra for the same doping level (See Figs. 9(a) and (b)). The Ca-insensitive behavior was also observed in the conductivity spectra and the dc conductivity values in Fig. 5. These facts imply that the Ca atoms in the Y-layer do not act as strong scattering centers for the carriers in the CuO_2 planes. The effect of disorders in the blocking layers was intensively discussed in terms of a weak scattering center in ref. 34. The Ca-substitution in the present system is considered to give a similar weak scattering effect.

This weak scattering is in sharp contrast to the strong scattering due to the in-plane disorder such as in Zn. Zn is a well-known impurity which causes pair-breaking in a d -wave superconductor. The strong Zn-effect can be seen in the radical reduction of superfluid density in Fig. 8, where the λ_L^{-2} estimated from the optical spectrum of Zn-substituted Y-123 (Y-123(Zn)) is also plotted [2]. Although T_c values are almost the same (87K and 85K) in optimally doped Y/Ca-123 and Y-123(Zn), the superfluid density is much smaller in Y-123(Zn) than in Y/Ca-123. Therefore, in the case of Ca-substitution, the T_c -suppression accompanied with the reduction in superfluid density and with the increase in unpaired carriers must be distinguished from the usual impurity pair-breaking in a d -wave superconductor. We need another mechanism to explain the T_c suppression without increasing residual resistivity. It should give the answer for the problem of the blocking layer effect on T_c .

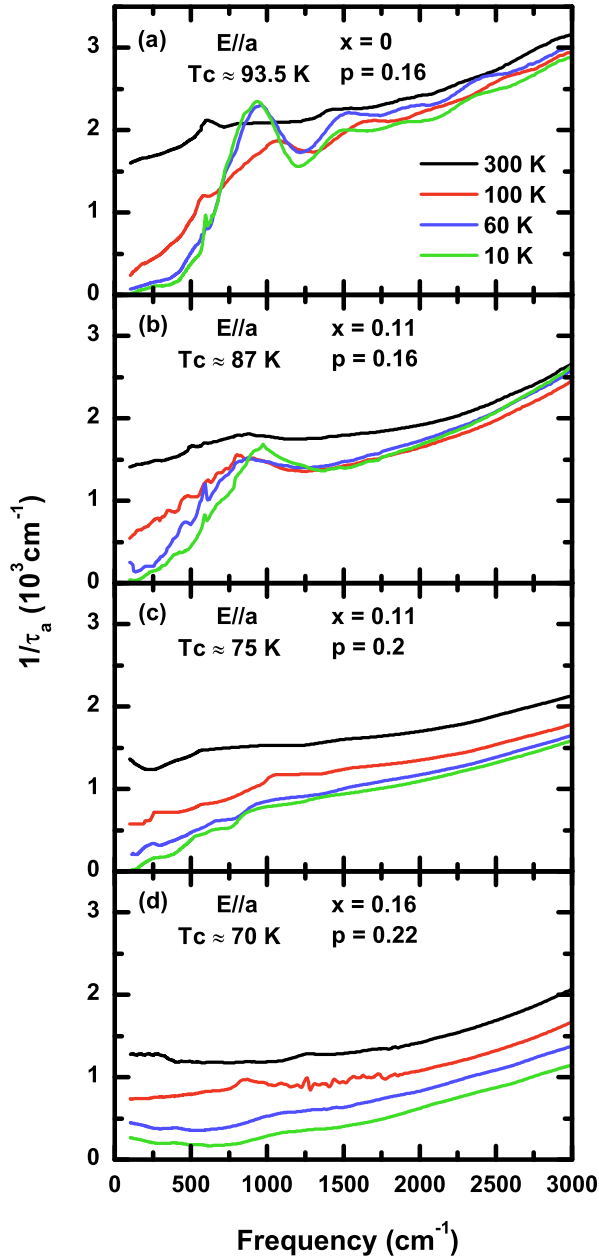


FIG. 9. Temperature dependent a-axis optical scattering rate in the optimally doped region for (a) $x = 0$ and (b) $x = 0.11$ and in the overdoped region for (c) $x = 0.11$, and (d) $x = 0.16$.

CONCLUSIONS

We performed temperature dependent measurements of in-plane reflectivity on detwinned $Y_{1-x}Ca_xB_2Cu_3O_{7-\delta}$ single crystals with various Ca and oxygen concentrations. In the heavily overdoped region, despite a small suppression of the optical con-

ductivity, a clear superconducting gap feature could not be observed because of the huge residual conductivity. The comparison of the spectra between optimally doped and heavily overdoped samples with the same Ca-contents showed that the residual conductivity increases with carrier-overdoping. Since we successfully removed the Ca-disorder effect in the experiment, we conclude that the increase of residual conductivity is an intrinsic property of the high temperature cuprate superconductors.

We also compared the Ca-substituted and Ca-free samples at the fixed doping level ($p = 0.16$) to observe the Ca-substitution effect on the residual conductivity. As a result, we found that the disorder effect due to Ca-substitution also causes the increase of the residual conductivity.

Most of the b -axis spectra are characterized by the mid-infrared absorption due to hopping conduction in the chain in addition to the plane response. Only for the heavily oxygenated Ca-free Y-123 sample, where the one-dimensional chain structure shows a highly ordered structure, the chain itself shows a suppression of conductivity below T_c . A possible reason for the superconducting chain behavior would be the proximity coupling effect of the chains with two-dimensional superconducting CuO_2 planes.

ACKNOWLEDGEMENTS

This work was supported by the New Energy and Industrial Technology Development Organization (NEDO), and the Grant-in-Aid for Scientific Research from the Ministry of Education, Culture, Sports, Science and Technology of Japan.

-
- [1] A. V. Puchkov, D. N. Basov, and T. Timusk, *J. Phys.: Condens. Matter* 8, 10049 (1996)
 - [2] N. L. Wang, S. Tajima, A. I. Rykov, and K. Tomimoto, *Phys. Rev. B* 57, R11081 (1998)
 - [3] D. B. Tanner and T. Timusk, *Physical Properties of High Temperature Superconductors III*, edited by D. M. Ginsberg (World Scientific, Singapore, 1992), p. 363
 - [4] J. Schützmann, S. Tajima, S. Miyamoto, and S. Tanaka, *Phys. Rev. Lett.* 73, 174 (1994)
 - [5] J. Schützmann, S. Tajima, S. Miyamoto, Y. Sato, and I. Terasaki, *Solid State Comm.* 94, 293 (1995)
 - [6] C. Bernhard, R. Henn, A. Wittlin, M. Kläser, Th. Wolf, G. Müller-Vogt, C. T. Lin, and M. Cardona, *Phys. Rev. Lett.* 80, 1762 (1998)
 - [7] Y. C. Ma and N. L. Wang, *Phys. Rev. B* 73, 144503 (2006)
 - [8] J. Hwang, T. Timusk, and G. D. Gu, *J. Phys.: Condens. Matter* 19, 125208 (2007)
 - [9] Y. Yamada and Y. Shiohara, *Physica C* 217, 182 (1993)

- [10] M. R. Presland, J. L. Tallon, R. G. Buckley, R. S. Liu, and N. E. Flower, *Physica C* 176, 95 (1991)
- [11] B. Fisher, J. Genossar, C. G. Kuper, L. Patlagan, G. M. Reisner, and A. Knizhnik, *Phys. Rev. B* 47, 6054 (1993)
- [12] L. D. Rotter, Z. Schlesinger, R. T. Collins, F. Holtzberg, C. Field, U. W. Welp, G. W. Crabtree, J. Z. Liu, Y. Fang, K. G. Vandervoort, and S. Fleshlert, *Phys. Rev. Lett.* 67, 2741 (1991)
- [13] D. N. Basov, R. Liang, B. Dabrowski, D. A. Bonn, W. N. Hardy, and T. Timusk, *Phys. Rev. Lett.*, 77, 4090 (1996)
- [14] D. N. Basov and T. Timusk, *Rev. Mod. Phys.* 77, 721 (2005)
- [15] J. J. Tu, C. C. Homes, G. D. Gu, D. N. Basov, and M. Strongin, *Phys. Rev. B* 66, 144514 (2002)
- [16] N. L. Wang, P. Zheng, J. L. Luo, Z. J. Chen, S. L. Yan, L. Fang, and Y. C. Ma, *Phys. Rev. B* 68, 054516 (2003)
- [17] D. N. Basov, R. Liang, D. A. Bonn, W. N. Hardy, B. Dabrowski, M. Quijada, D. B. Tanner, J. P. Rice, D. M. Ginsberg, and T. Timusk, *Phys. Rev. Lett.* 74, 598 (1995)
- [18] Z. Schlesinger, R. T. Collins, F. Holtzberg, C. Feild, S. H. Blanton, U. Welp, G. W. Crabtree, Y. Fang, and J. Z. Liu *Phys. Rev. Lett.* 65, 801 (1990)
- [19] J. Schützmann, B. Gorshunov, K. F. Renk, J. Münzel, A. Zibold, H. P. Geserich, A. Erb, and G. Müller-Vogt, *Phys. Rev. B* 46, 512 (1992)
- [20] V. Z. Kresin and S. A. Wolf, *Phys. Rev. B* 46, 6458 (1992)
- [21] Y. -S. Lee, K. Segawa, Y. Ando, and D. N. Basov, *Phys. Rev. Lett.* 94, 137004 (2005)
- [22] M. Dumm, S. komiya, Y. Ando, and D. N. Basov, *Phys. Rev. Lett.* 91, 077004 (2003)
- [23] Y. -S. Lee, K. Segawa, Y. Ando, and D. N. Basov, *Phys. Rev. B* 70, 014518 (2004)
- [24] D. N. Basov, R. Liang, D. A. Bonn, W. N. Hardy, B. Dabrowski, M. Quijada, D. B. Tanner, J. P. Rice, D. M. Ginsberg, and T. Timusk, *Phys. Rev. Lett.* 74, 598 (1995)
- [25] Ch. Niedermayer, C. Bernhard, U. Binniger, H. Glükler, J. L. Tallon, E. J. Ansaldo, and J. I. Budnick, *Phys. Rev. Lett.* 71, 1764 (1993)
- [26] Y. J. Uemura, A. Keren, L. P. Le, G. M. Luke, W. D. Wu, Y. Kubo, T. Manako, Y. Shimakawa, M. Subramanian, J. L. Cobbs, and J. T. Markert, *Nature* 364, 605 (1993)
- [27] J. L. Tallon, C. Bernhard, U. Binniger, A. Hofer, G. V. M. Williams, E. J. Ansaldo, J. I. Budnick, and Ch. Niedermayer, *Phys. Rev. Lett.* 74, 1008 (1995)
- [28] H. Mashima, N. Fukuo, Y. Matsumoto, G. Kinoda, T. Kondo, H. Ikuta, T. Hitosugi, and T. Hasegawa, *Phys. Rev. B* 73, 060502R (2006)
- [29] K. Kudo, T. Nishizaki, N. Okumura, and N. Kobayashi, 25th International Conference on Low Temperature Physics, *Journal of Physics: Conference Series* 150, 052133 (2009)
- [30] J. W. Loram, K. A. Mirza, J. M. Wade, J. R. Cooper, and W. Y. Liang, *Physica C* 235, 134 (1994)
- [31] K. Magishi, Y. Kitaoka, G.-q. Zheng, K. Asayama, T. Kondo, Y. Shimakawa, T. Manako, and Y. Kubo, *Phys. Rev. B* 54, 10131 (1996)
- [32] Y. Tanabe, T. Adachi, T. Noji, and Y. Koike, *J. Phys. Soc. Jpn.* 74, 2893 (2005)
- [33] J. Hwang, T. Timusk, and G. D. Gu, *Nature* 427, 714 (2004)
- [34] K. Fujita, T. Noda, K. M. Kojima, H. Eisaki, and S. Uchida, *Phys. Rev. Lett.* 95, 097006 (2005)